Observation of an Inner-Shell Orbital Clock Transition in Neutral Ytterbium Atoms

Taiki Ishiyama, Koki Ono,[*] Tetsushi Takano, Ayaki Sunaga, and Yoshiro Takahashi

Department of Physics, Graduate School of Science, Kyoto University, Kyoto 606-8502, Japan

We observe a weakly allowed optical transition of atomic ytterbium from the ground state to the metastable state $4f^{13}5d6s^2$ ($J = 2$) for all five bosonic and two fermionic isotopes with resolved Zeeman and hyperfine structures. This inner-shell orbital transition has been proposed as a new frequency standard as well as a quantum sensor for new physics. We find magic wavelengths through the measurement of the scalar and tensor polarizabilities and reveal that the measured trap lifetime in a three-dimensional optical lattice is 1.9(1) s, which is crucial for precision measurements. We also determine the g factor by an interleaved measurement, consistent with our relativistic atomic calculation. This work opens the possibility of an optical lattice clock with improved stability and accuracy as well as novel approaches for physics beyond the standard model.

Recent development of optical atomic clocks using ions and neutral atoms has established a high fractional accuracy at the 10^{-18} level [1–3]. In addition to the contribution to metrology such as the redefinition of the second [4,5] and geodesy [6,7], a highly stable atomic clock enables various applications ranging from quantum simulations [8,9] to fundamental physics [10] including gravitational wave detection [11], and others. The development of even more precise clocks benefits all of these applications.

Recently, the optical transition of atomic ytterbium (Yb) to its metastable state $4f^{13}5d6s^2$ ($J = 2$) with an energy of 23 188.518 cm^{-1} [12] has been proposed as a new frequency standard with high stability and accuracy [13,14]. As shown in Fig. 1, the radiative lifetime of the $4f^{13}5d6s^2$ ($J = 2$) state is calculated to be much longer than that of the other metastable states, which potentially improves the quality factor of an optical lattice clock. In addition, the quadratic Zeeman shift as well as the black-body-radiation shift of the $^1S_0 \leftrightarrow 4f^{13}5d6s^2$ ($J = 2$) transition are calculated to be considerably small compared to those of the $^1S_0 \leftrightarrow {}^3P_0$ and $^1S_0 \leftrightarrow {}^3P_2$ transitions [14], suggesting that the inner-shell orbital clock transition has a potential to reduce systematic uncertainties. The dual clock operation [15] combined with the well-established $^1S_0 \leftrightarrow {}^3P_0$ transition, or already observed $^1S_0 \leftrightarrow {}^3P_2$ transition [16] of Yb atoms, possibly can further reduce systematic uncertainties in a clock comparison.

This metastable state of Yb also attracts considerable interest from the viewpoints of new physics searches [13,14,17]. The $^3P_0 \leftrightarrow 4f^{13}5d6s^2$ ($J = 2$) as well as $^3P_2 \leftrightarrow 4f^{13}5d6s^2$ ($J = 2$) [18] transitions show some of the highest sensitivities in neutral atoms to the variation of the fine-structure constant, providing also the possibilities of searching for ultralight scalar dark matter [19] and

testing Einstein's equivalence principle [10]. The metastable state has also high sensitivity to the violation of local Lorentz invariance in the electron-photon sector [17,20], so far studied using single or two ions [21–24] and dysprosium atoms [25]. Furthermore, establishing a new clock transition associated with the metastable state, in addition to the $^1S_0 \leftrightarrow {}^3P_0$ and $^1S_0 \leftrightarrow {}^3P_2$ transitions, provides a unique possibility to study a nonlinearity of the King plot using five bosonic isotopes of Yb in the search for a hypothetical particle mediating a force between electrons and neutrons beyond the standard model [26,27]. Clearly, the first step toward these experiments is to experimentally observe the associated transition and characterizations such as the lifetime [13,14,18] and possible existence of a magic wavelength [14,18].

In this Letter, we report the observation of the $^1S_0 \leftrightarrow 4f^{13}5d6s^2$ ($J = 2$) optical transition of Yb. The resonances for all five bosonic and two fermionic isotopes are clearly
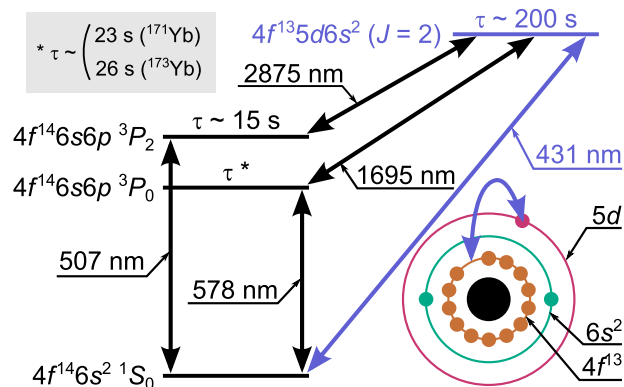

FIG. 1. Clock transitions in a Yb atom. The relevant transition wavelengths and lifetimes τ [14] are shown.

observed with resolved Zeeman and hyperfine structures. We find two magic wavelengths of 797.2(4) and 834.2(1) nm for the practical condition of $m_J = 0$ and the laser polarization perpendicular to a magnetic field, through the measurement of the polarizability. Here m_J is the projection of the total electronic angular momentum J along the quantization axis. In addition, our excitation and deexcitation sequence measurement of atoms in a three-dimensional optical lattice enables us to obtain the trap lifetime to be 1.9(1) s. Through an interleaved measurement with different magnetic fields, we determine the g factor to be 1.463(4), consistent with our relativistic many-body calculation. These findings are promising for the development of an optical lattice clock with improved stability and accuracy, and its various applications for searching for physics beyond the standard model.

Experimental setup.—All spectroscopic measurements other than the lifetime measurement are done using ultracold Yb atoms evaporatively cooled in a crossed far-off resonance trap (see Sec. S1 in Supplemental Material [28]). The number of atoms is about $2 \times 10^4 - 1.3 \times 10^5$ and the temperature is about $0.3 - 1$ μK, depending on the isotope. We apply a linearly polarized excitation light beam at a wavelength of 431 nm. We measure the number of atoms remaining in the ground state after the irradiation of the excitation laser, and identify the optical resonance through the resonant atom loss. The angle of linear polarization, light intensity, and irradiation time are adjusted to optimize each spectroscopic measurement. We note that the lifetime measurement is done for atoms loaded into a three-dimensional (3D) optical lattice.

Zeeman and hyperfine spectra.—Figure 2 summarizes the isotope shifts, Zeeman, and hyperfine spectra of the five bosonic isotopes (^{168}Yb, ^{170}Yb, ^{172}Yb, ^{174}Yb, and ^{176}Yb with nuclear spin $I = 0$) and the two fermionic isotopes (^{171}Yb and ^{173}Yb, with $I = 1/2$ and $5/2$, respectively). The upper panel of Fig. 2(a) shows the spectra of the five bosonic isotopes, and the lower panel shows m_J-resolved spectra of ^{174}Yb. The angle between the propagation (polarization) direction of the excitation light and the quantization axis, defined by a magnetic field, is 45° (24°). This configuration allows the excitation to all magnetic sublevels of the $4f^{13}5d6s^2$ ($J = 2$) state, according to the selection rule for a magnetic quadrupole ($M2$) transition. The typical full width at half maximum (FWHM) is about 30 kHz, limited by the Doppler broadening of about 20 kHz and the finite laser linewidth of about 10 kHz. Note that more than half of the atoms are lost at the peak, suggesting some atom loss mechanism in the $4f^{13}5d6s^2$ ($J = 2$) state, possibly caused by a shallow trapping potential and inelastic atom collisions.

Successful observation of the spectra of all bosonic isotopes enables us to determine the isotope shifts of the $^1S_0 \leftrightarrow 4f^{13}5d6s^2$ ($J = 2$) transition (see Sec. S2 in Supplemental Material [28]). The determined isotope shifts are summarized in Table I, where only the statistical errors
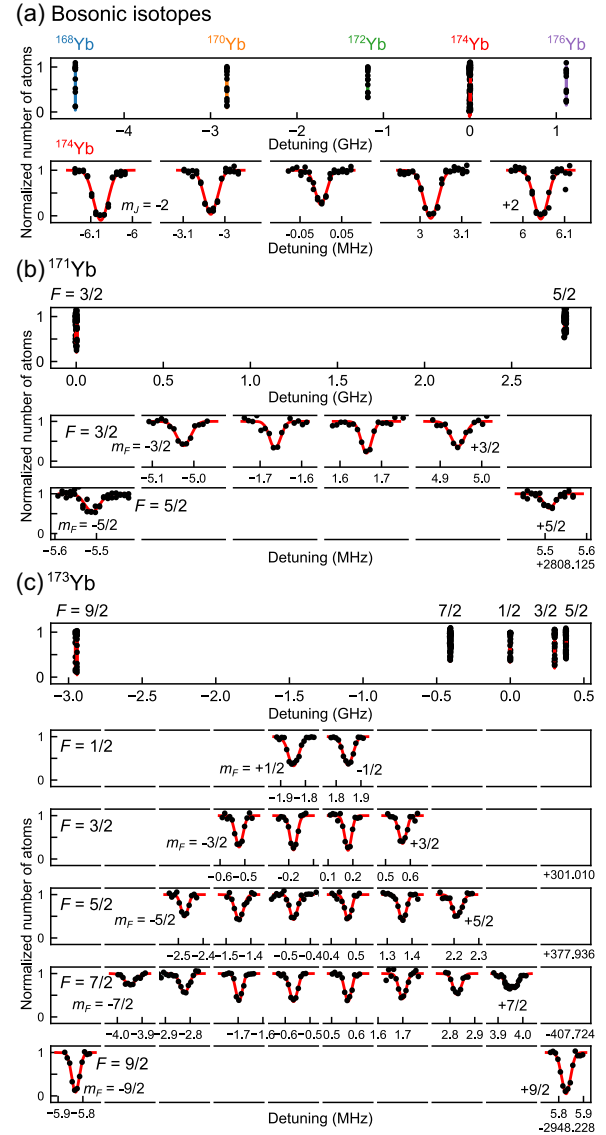

FIG. 2. Excitation spectra of all stable isotopes. (a) Five bosonic isotopes. The upper figure shows all spectra of the five isotopes for $m_J = 0$ state, except for ^{174}Yb, and the lower shows a magnified view around ^{174}Yb. The horizontal axis is the detuning from the resonance frequency of ^{174}Yb ($m_J = 0$). (b),(c) Two fermionic isotopes, (b) ^{171}Yb($I = 1/2$) and (c) ^{173}Yb($I = 5/2$). The top figures show all spectra of all hyperfine states, and the lower show m_F-resolved spectra of each hyperfine state. The horizontal axis is the detuning from the average of $m_F = \pm 1/2$ in $F = 3/2$ for ^{171}Yb and $F = 1/2$ for ^{173}Yb. The solid curves are the fits with a Gaussian function. Note that not all the magnetic sublevels for $F = 5/2$ (9/2) state of ^{171}Yb (^{173}Yb) are shown.

are evaluated. Note that many systematic effects, such as the light shift and the quadratic Zeeman shift, are common among the isotopes within the accuracy of the present measurement. In order to evaluate a possible line shift due to s-wave collisions between trapped ultracold atoms, which would be the largest systematic effect among many, we perform interleaved measurements with two different

TABLE I. Measured isotope shifts $\nu^{A'A} := \nu^{A'} - \nu^A$ of the $4f^{14}6s^2\,^1S_0 \leftrightarrow 4f^{13}5d6s^2$ $(J=2)$ transition, where ν^A is the transition frequency of a Yb isotope with a mass number A. Statistical 1σ uncertainties are shown as $(\cdot)_{\text{stat}}$.

Isotope pair (A', A)	Isotope shift $\nu^{A'A}$ (MHz)
(168,174)	$-4564.596(2)_{\text{stat}}$
(170,174)	$-2810.666(2)_{\text{stat}}$
(172,174)	$-1180.614(2)_{\text{stat}}$
(174,176)	$-1115.766(6)_{\text{stat}}$

numbers of atoms by adjusting the evaporative cooling process. For the five bosonic isotopes, the resonance shifts, corrected for the difference in the atomic temperature, are within the uncertainties of about 5 kHz, and we find no evidence of atomic collision shifts at our measurement conditions.

In addition, we precisely determine the g factor of the $4f^{13}5d6s^2$ $(J=2)$ state as $g_J = 1.463(4)$ with the uncertainty determined by the propagation of the fitting error and the uncertainty of the magnetic field calibration (see Sec. S3 in Supplemental Material [28]). Our theoretical calculation of the g factor using the DIRAC program [29,30] gives $g_J = 1.465(2)$, which is consistent with the experiment (see Sec. S7 in Supplemental Material [28]).

Figures 2(b) and 2(c) show the hyperfine (top panel) and Zeeman spectra (lower panels) of ^{171}Yb and ^{173}Yb, respectively. The observed Zeeman spectra for fermionic isotopes are well explained by the measured g_J. Here, we identify an excitation mechanism other than the $M2$ transition. A hyperfine interaction can cause the $4f^{13}5d6s^2$ $(J=2)$ state to mix with other states such as $^3P_1$ and $4f^{13}5d6s^2$ $(J=1)$ states, making the electric-dipole ($E1$) transition partially allowed, which is called a hyperfine-induced $E1$ transition [31]. The transition to the $F=3/2$ state of ^{171}Yb and those to the $F=3/2, 5/2$, and $7/2$ of ^{173}Yb are $E1$ allowed, and give resonance signals much stronger than other transitions that are allowed only by $M2$.

The data shown in Figs. 2(b) and 2(c) enable us to determine the hyperfine constants of ^{171}Yb and ^{173}Yb of the $4f^{13}5d6s^2$ $(J=2)$ state, respectively (see Sec. S4 in Supplemental Material [28]). We obtain the magnetic dipole constant $A_{\text{hfs}}(^{171}\text{Yb}) = 1123.3(3)$ MHz, and $A_{\text{hfs}}(^{173}\text{Yb}) = -309.46(4)$ MHz, and the electric quadrupole constant $B_{\text{hfs}}(^{173}\text{Yb}) = -1700.6(9)$ MHz, with the uncertainties due to the fitting error. Note that the presumably much smaller systematic effects such as the collision shift are not evaluated at present. The careful evaluation of the systematic effects and precise determination of the hyperfine constants will be an important future work. It is also noted that introducing a magnetic octupole constant C_{hfs} for ^{173}Yb does not improve the fitting.

Differential polarizability.—We perform a measurement of the wavelength-dependent polarizability of the $4f^{13}5d6s^2$ $(J=2)$ state. This is very important in the search for a magic wavelength at which the polarizabilities of the ground and $4f^{13}5d6s^2$ $(J=2)$ states coincide, and thus the line shift due to the trapping light is largely suppressed, enabling ultranarrow-linewidth spectroscopy and accurate clock operation [32].

In the case of linear polarization, the total polarizability α of the state $|J, m_J\rangle$ is

$$\alpha = \alpha^S + \frac{3\cos^2\theta - 1}{2}\frac{3m_J^2 - J(J+1)}{J(2J-1)}\alpha^T, \qquad (1)$$

where the superscripts S and T denote scalar and tensor, respectively, and θ is the polarization angle with respect to the quantization axis [33]. Using this formula, the differential polarizability $\Delta\alpha$ between the ground state with $J=0$ and the $4f^{13}5d6s^2$ $(J=2)$ state is given in a straightforward manner.

In this Letter, we search for a magic wavelength within the tunable range of a Ti:sapphire laser which can provide enough power for optical lattices (see Sec. S5B in Supplemental Material [28]). In particular, in this wavelength range, there are two $E1$-allowed optical transitions of $4f^{13}5d6s^2 (J=2) \leftrightarrow 4f^{13}6s^26p_{3/2}(J=3)$ at a wavelength of 792.5 nm and $4f^{13}5d6s^2(J=2) \leftrightarrow 4f^{13}6s^26p_{3/2}(J=2)$ at 832.7 nm [12], which will resonantly change the polarizability. In fact, according to our calculation for the excited state and Ref. [34] for the ground state, the magic wavelengths are expected to be around 795.5 and 833.7 nm for $m_J = 0$ and $\theta = 90°$ (see Sec. S5A in Supplemental Material [28]).

As shown in Figs. 3(a) and 3(b), we observe the resonant changes of the polarizability in the vicinity of the transition wavelengths of 792.5 and 832.7 nm. The solid curves are the fits to the data using the following equation: $\Delta\alpha(\omega) = a/(\omega_0^2 - \omega^2) + b$, where a and b are fitting parameters, ω is the angular frequency of a Ti:sapphire laser, and ω_0 is the resonance angular frequency of the $4f^{13}5d6s^2 (J=2) \leftrightarrow 4f^{13}6s^26p_{3/2}(J=3)$ or $4f^{13}5d6s^2(J=2) \leftrightarrow 4f^{13}6s^26p_{3/2}(J=2)$ transition, given in Ref. [12]. Note that this model assumes that only one resonant transition with ω_0 dominantly contributes to the wavelength dependence, while the effects of other off-resonant transitions contribute as wavelength-independent offset constant b. From the fitting, we can determine the magic wavelengths λ_{magic} as follows:

$$\lambda_{\text{magic}} = \begin{cases} 798.9(4) \text{ nm} & (m_J = 0, \theta = 0°) \\ \left.\begin{array}{l}797.2(4) \text{ nm} \\ 834.2(1) \text{ nm}\end{array}\right\} & (m_J = 0, \theta = 90°) \\ 833.28(4) \text{ nm} & (m_J = 2, \theta = 90°). \end{cases} \qquad (2)$$

Since two measurements with different θ or m_J at each wavelength are performed, we can determine the differential scalar polarizability $\Delta\alpha^S$ and the tensor polarizability
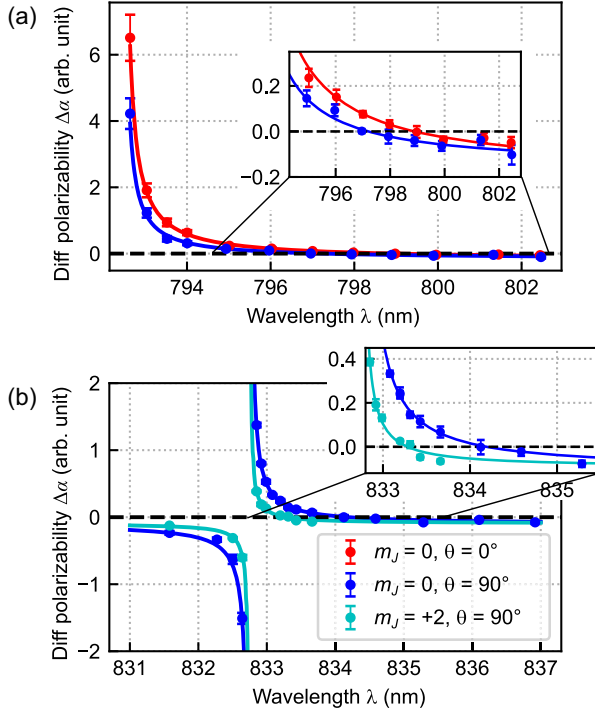
FIG. 3. Differential polarizability measurement between $^1S_0$ and $4f^{13}5d6s^2$ $(J = 2)$ states. Measurements around the transitions: (a) $4f^{13}5d6s^2(J = 2) \leftrightarrow 4f^{13}6s^26p_{3/2}(J = 3)$ at 792.5 nm and (b) $4f^{13}5d6s^2(J = 2) \leftrightarrow 4f^{13}6s^26p_{3/2}(J = 2)$ at 832.7 nm. The differential polarizability, shown on the vertical axis as arbitrary units, is obtained from the linear fit to the measured differential light shifts $\Delta\nu$ as a function of the Ti: sapphire laser intensity. The error bars on the vertical axis are obtained from the error propagation of the standard error of $\Delta\nu$ and the uncertainty of the Ti:sapphire laser intensity. The solid curves are fits to the data.

α^T from Eq. (1). Possible trap geometries to minimize the uncertainty of the tensor light shift on the performance of clock operation using the 797.2 nm optical lattice are discussed in Sec. S5C of Supplemental Material [28]. It should be noted that the differential higher-order light shift due to $M1$ and $E2$ multipolar polarizabilities and $E1$ hyperpolarizability [35] should exist even at an $E1$ magic wavelength, where the differential light shift due to $E1$ polarizability vanishes [32]. The investigation of the operational magic condition for wavelength and intensity, where the overall light shift is insensitive to the lattice-intensity variation [36], will be an important future work for clock operation.

Lifetime.—The lifetime of the excited state of a clock transition is important because it is directly related to the quality factor of the clock transition. In this measurement, we use spin-polarized ^{173}Yb atoms in the $|F = 5/2,$ $m_F = 5/2\rangle$ state loaded into a 3D optical lattice to minimize the possible atom loss due to inelastic interatomic collisions. The 3D optical lattice consists of a 2D optical lattice at the wavelength $\lambda_1 = 759.4$ nm and a 1D optical
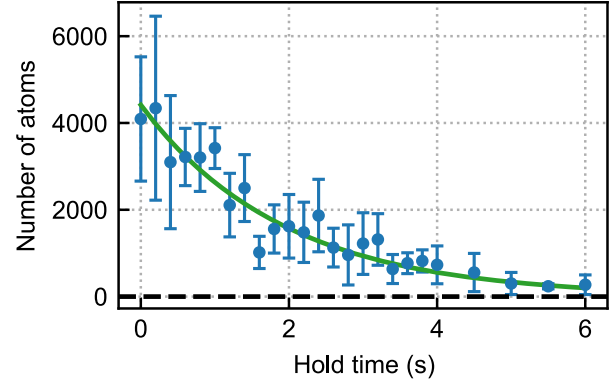

FIG. 4. Lifetime measurement of atoms in $4f^{13}5d6s^2$ $(J = 2)$ state. The horizontal axis shows the time to hold the excited atoms in the optical lattice, and the vertical axis shows the number of atoms in the excited state after the hold time. The measurements are repeated 4 times, and the mean and standard deviation are plotted.

lattice at the wavelength $\lambda_2 = 797.2$ nm, superimposed on the excitation light (see Sec. S6 in Supplemental Material [28]). Figure 4 shows the number of excited atoms as a function of the holding time in the optical lattice. The lattice depths are $28E_R$ for the 2D optical lattice at λ_1 and $25E_R$ for the 1D optical lattice at λ_2. Here $E_R = h^2/(2m\lambda_2^2) = h \times 1.8$ kHz represents the recoil energy at the wavelength λ_2, where h is the Planck constant and m is the mass of a Yb atom. From the fit to the data with a single exponential function, the trap lifetime of the excited atoms is obtained as 1.9(1) s. As a reference, we also investigate the trap loss of atoms in the ground state $^1S_0$ in the same experimental setup, and find the trap lifetime to be 2.8(2) s, which would be limited by some mechanism such as collisions with background gases. Assuming that the same mechanism also limits the trap lifetime of the $4f^{13}5d6s^2$ $(J = 2)$ state, we infer the intrinsic state lifetime of the excited state to be 5.9(1.3) s. This is compared with the theoretical calculations in Refs. [13,14,18], which predict a lifetime of about 60, 200, and 190 s, respectively. Our preliminary estimation shows that the rate of the photon scattering γ_{sc} due to the lattice laser beam of near resonant 797.2 nm light at $25E_R$ is $\gamma_{sc} = 0.15$ s^{-1}, which seemingly explains the measured result. Further systematic measurements with various experimental conditions will clarify the intrinsic lifetime of this state.

Summary.—We report the observation of the $^1S_0 \leftrightarrow$ $4f^{13}5d6s^2$ $(J = 2)$ optical transition of all seven Yb isotopes with resolved Zeeman and hyperfine structures. Two magic wavelengths of 797.2(4) and 834.2(4) nm for practical conditions are found and the measured lifetime is 1.9(1) s, promising for applications for precision measurements. We also determine the g factor to be 1.463(4), and compare the result with our relativistic many-body

calculation with good agreement. A 3D optical lattice experiment with many ultracold atoms with isotope mixtures for the observed $4f^{13}5d6s^2$ ($J = 2$) state is promising to test the violation of local Lorentz invariance of electron-photon sector and Einstein's weak equivalence principle.

---

*koukiono3@yagura.scphys.kyoto-u.ac.jp

[1] C. W. Chou, D. B. Hume, J. C. J. Koelemeij, D. J. Wineland, and T. Rosenband, Frequency Comparison of Two High-Accuracy Al⁺ Optical Clocks, Phys. Rev. Lett. **104**, 070802 (2010).

[2] B. J. Bloom, T. L. Nicholson, J. R. Williams, S. L. Campbell, M. Bishof, X. Zhang, W. Zhang, S. L. Bromley, and J. Ye, An optical lattice clock with accuracy and stability at the 10^{-18} level, Nature (London) **506**, 71 (2014).

[3] I. Ushijima, M. Takamoto, M. Das, T. Ohkubo, and H. Katori, Cryogenic optical lattice clocks, Nat. Photonics **9**, 185 (2015).

[4] C. Grebing, A. Al-Masoudi, S. Dörscher, S. Häfner, V. Gerginov, S. Weyers, B. Lipphardt, F. Riehle, U. Sterr, and C. Lisdat, Realization of a timescale with an accurate optical lattice clock, Optica **3**, 563 (2016).

[5] W. R. Milner, J. M. Robinson, C. J. Kennedy, T. Bothwell, D. Kedar, D. G. Matei, T. Legero, U. Sterr, F. Riehle, H. Leopardi *et al.*, Demonstration of a Timescale Based on a Stable Optical Carrier, Phys. Rev. Lett. **123**, 173201 (2019).

[6] T. Takano, M. Takamoto, I. Ushijima, N. Ohmae, T. Akatsuka, A. Yamaguchi, Y. Kuroishi, H. Munekane, B. Miyahara, and H. Katori, Geopotential measurements with synchronously linked optical lattice clocks, Nat. Photonics **10**, 662 (2016).

[7] C. Lisdat, G. Grosche, N. Quintin, C. Shi, S. M. F. Raupach, C. Grebing, D. Nicolodi, F. Stefani, A. Al-Masoudi, S. Dörscher *et al.*, A clock network for geodesy and fundamental science, Nat. Commun. **7**, 12443 (2016).

[8] S. Kato, K. Inaba, S. Sugawa, K. Shibata, R. Yamamoto, M. Yamashita, and Y. Takahashi, Laser spectroscopic probing of coexisting superfluid and insulating states of an atomic Bose–Hubbard system, Nat. Commun. **7**, 11341 (2016).

[9] S. Kolkowitz, S. L. Bromley, T. Bothwell, M. L. Wall, G. E. Marti, A. P. Koller, X. Zhang, A. M. Rey, and J. Ye,

Spin–orbit-coupled fermions in an optical lattice clock, Nature (London) **542**, 66 (2017).

[10] M. S. Safronova, D. Budker, D. DeMille, Derek F. Jackson Kimball, A. Derevianko, and C. W. Clark, Search for new physics with atoms and molecules, Rev. Mod. Phys. **90**, 025008 (2018).

[11] S. Kolkowitz, I. Pikovski, N. Langellier, M. D. Lukin, R. L. Walsworth, and J. Ye, Gravitational wave detection with optical lattice atomic clocks, Phys. Rev. D **94**, 124043 (2016).

[12] A. Kramida, Y. Ralchenko, J. Reader, and NIST ASD Team, NIST Atomic Spectra Database (version 5.10), https://physics.nist.gov/asd.

[13] M. S. Safronova, S. G. Porsev, C. Sanner, and J. Ye, Two Clock Transitions in Neutral Yb for the Highest Sensitivity to Variations of the Fine-Structure Constant, Phys. Rev. Lett. **120**, 173001 (2018).

[14] V. A. Dzuba, V. V. Flambaum, and S. Schiller, Testing physics beyond the standard model through additional clock transitions in neutral ytterbium, Phys. Rev. A **98**, 022501 (2018).

[15] D. Akamatsu, T. Kobayashi, Y. Hisai, T. Tanabe, K. Hosaka, M. Yasuda, and F.-L. Hong, Dual-mode operation of an optical lattice clock using strontium and ytterbium atoms, IEEE Trans. Ultrason. Ferroelectr. Freq. Control **65**, 1069 (2018).

[16] A. Yamaguchi, S. Uetake, S. Kato, H. Ito, and Y. Takahashi, High-resolution laser spectroscopy of a Bose–Einstein condensate using the ultranarrow magnetic quadrupole transition, New J. Phys. **12**, 103001 (2010).

[17] R. Shaniv, R. Ozeri, M. S. Safronova, S. G. Porsev, V. A. Dzuba, V. V. Flambaum, and H. Häffner, New Methods for Testing Lorentz Invariance with Atomic Systems, Phys. Rev. Lett. **120**, 103202 (2018).

[18] Z.-M. Tang, Y.-m. Yu, B. K. Sahoo, C.-Z. Dong, Y. Yang, and Y. Zou, A new clock transition with the highest sensitivity to α variation and simultaneous magic trapping conditions with other clock transitions in Yb, arXiv:2208.09200.

[19] A. Arvanitaki, J. Huang, and K. Van Tilburg, Searching for dilaton dark matter with atomic clocks, Phys. Rev. D **91**, 015015 (2015).

[20] V. A. Kostelecký and C. D. Lane, Constraints on Lorentz violation from clock-comparison experiments, Phys. Rev. D **60**, 116010 (1999).

[21] T. Pruttivarasin, M. Ramm, S. G. Porsev, I. I. Tupitsyn, M. S. Safronova, M. A. Hohensee, and H. Häffner, Michelson–Morley analogue for electrons using trapped ions to test Lorentz symmetry, Nature (London) **517**, 592 (2015).

[22] E. Megidish, J. Broz, N. Greene, and H. Häffner, Improved Test of Local Lorentz Invariance from a Deterministic Preparation of Entangled States, Phys. Rev. Lett. **122**, 123605 (2019).

[23] C. Sanner, N. Huntemann, R. Lange, C. Tamm, E. Peik, M. S. Safronova, and S. G. Porsev, Optical clock comparison for Lorentz symmetry testing, Nature (London) **567**, 204 (2019).

[24] L. S. Dreissen, C.-H. Yeh, H. A. Fürst, K. C. Grensemann, and T. E. Mehlstäubler, Improved bounds on Lorentz

violation from composite pulse Ramsey spectroscopy in a trapped ion, Nat. Commun. **13**, 7314 (2022).

[25] M. A. Hohensee, H. Müller, and R. B. Wiringa, Equivalence Principle and Bound Kinetic Energy, Phys. Rev. Lett. **111**, 151102 (2013).

[26] J. C. Berengut, D. Budker, C. Delaunay, V. V. Flambaum, C. Frugiuele, E. Fuchs, C. Grojean, R. Harnik, R. Ozeri, G. Perez, and Y. Soreq, Probing New Long-Range Interactions by Isotope Shift Spectroscopy, Phys. Rev. Lett. **120**, 091801 (2018).

[27] K. Ono, Y. Saito, T. Ishiyama, T. Higomoto, T. Takano, Y. Takasu, Y. Yamamoto, M. Tanaka, and Y. Takahashi, Observation of Nonlinearity of Generalized King Plot in the Search for New Boson, Phys. Rev. X **12**, 021033 (2022).

[28] See Supplemental Material at http://link.aps.org/supplemental/10.1103/PhysRevLett.130.153402, which includes Refs. [14,27,29–31,33,34,37–54], for details of the experimental system (Sec. S1), details of the measurement procedures (Secs. S2, S3, S5B, and S6), details of the analysis (Sec. S4), details of the theoretical calculations (Secs. S5A and S7), and discussion (Sec. S5C).

[29] T. Saue, R. Bast, A. S. P. Gomes, H. J. A. Jensen, L. Visscher, I. A. Aucar, R. Di Remigio, K. G. Dyall, E. Eliav, E. Fasshauer *et al.*, The DIRAC code for relativistic molecular calculations, J. Chem. Phys. **152**, 204104 (2020).

[30] H. J. Aa. Jensen, R. Bast, A. S. P. Gomes, T. Saue, L. Visscher *et al.*, DIRAC, A relativistic *ab initio* electronic structure program, release DIRAC22, 10.5281/zenodo.6010450; see also http://www.diracprogram.org, accessed 2022; see also http://www.diracprogram.org.

[31] M. M. Boyd, T. Zelevinsky, A. D. Ludlow, S. Blatt, T. Zanon-Willette, S. M. Foreman, and J. Ye, Nuclear spin effects in optical lattice clocks, Phys. Rev. A **76**, 022510 (2007).

[32] H. Katori, M. Takamoto, V. G. Pal'chikov, and V. D. Ovsiannikov, Ultrastable Optical Clock with Neutral Atoms in an Engineered Light Shift Trap, Phys. Rev. Lett. **91**, 173005 (2003).

[33] F. Le Kien, P. Schneeweiss, and A. Rauschenbeutel, Dynamical polarizability of atoms in arbitrary light fields: General theory and application to cesium, Eur. Phys. J. D **67**, 92 (2013).

[34] Z.-M. Tang, Y.-M. Yu, J. Jiang, and C.-Z. Dong, Magic wavelengths for the transition in ytterbium atom, J. Phys. B **51**, 125002 (2018).

[35] S. G. Porsev, M. S. Safronova, U. I. Safronova, and M. G. Kozlov, Multipolar Polarizabilities and Hyperpolarizabilities in the Sr Optical Lattice Clock, Phys. Rev. Lett. **120**, 063204 (2018).

[36] I. Ushijima, M. Takamoto, and H. Katori, Operational Magic Intensity for Sr Optical Lattice Clocks, Phys. Rev. Lett. **121**, 263202 (2018).

[37] S. Taie, Y. Takasu, S. Sugawa, R. Yamazaki, T. Tsujimoto, R. Murakami, and Y. Takahashi, Realization of a SU(2) × SU(6) System of Fermions in a Cold Atomic Gas, Phys. Rev. Lett. **105**, 190401 (2010).

[38] X. Baillard, A. Gauguet, S. Bize, P. Lemonde, P. Laurent, A. Clairon, and P. Rosenbusch, Interference-filter-stabilized external-cavity diode lasers, Opt. Commun. **266**, 609 (2006).

[39] R. W. P. Drever, J. L. Hall, F. V. Kowalski, J. Hough, G. M. Ford, A. J. Munley, and H. Ward, Laser phase and frequency stabilization using an optical resonator, Appl. Phys. B **31**, 97 (1983).

[40] B. Budick and J. Snir, g_j values of excited states of the ytterbium atom, Phys. Lett. A **24**, 689 (1967).

[41] M. Baumann and G. Wandel, g_j factors of the $6s6p\,^3P_1$ and $6s6p\,^1P_1$ states of ytterbium, Phys. Lett. A **28**, 200 (1968).

[42] C. Schwartz, Theory of hyperfine structure, Phys. Rev. **97**, 380 (1955).

[43] L. Olschewski, Messung der magnetischen Kerndipolmomente an freien ^{43}Ca-, ^{87}Sr-, ^{135}Ba-, ^{137}Ba-, ^{171}Yb- und ^{173}Yb-Atomen mit optischem Pumpen, Z. Phys. **249**, 205 (1972).

[44] N. J. Stone, Table of nuclear magnetic dipole and electric quadrupole moments, At. Data Nucl. Data Tables **90**, 75 (2005).

[45] S. G. Porsev, A. Derevianko, and E. N. Fortson, Possibility of an optical clock using the $6^1S_0 \rightarrow 6^3P_0^o$ transition in ^{171,173}Yb atoms held in an optical lattice, Phys. Rev. A **69**, 021403(R) (2004).

[46] A. V. Taichenachev, V. I. Yudin, C. W. Oates, C. W. Hoyt, Z. W. Barber, and L. Hollberg, Magnetic Field-Induced Spectroscopy of Forbidden Optical Transitions with Application to Lattice-Based Optical Atomic Clocks, Phys. Rev. Lett. **96**, 083001 (2006).

[47] T. Akatsuka, M. Takamoto, and H. Katori, Optical lattice clocks with non-interacting bosons and fermions, Nat. Phys. **4**, 954 (2008).

[48] M. Takamoto, F.-L. Hong, R. Higashi, Y. Fujii, M. Imae, and H. Katori, Improved frequency measurement of a one-dimensional optical lattice clock with a spin-polarized fermionic ^{87}Sr isotope, J. Phys. Soc. Jpn. **75**, 104302 (2006).

[49] A. W. Young, W. J. Eckner, W. R. Milner, D. Kedar, M. A. Norcia, E. Oelker, N. Schine, J. Ye, and A. M. Kaufman, Half-minute-scale atomic coherence and high relative stability in a tweezer clock, Nature (London) **588**, 408 (2020).

[50] K. G. Dyall and A. S. Gomes, Revised relativistic basis sets for the 5d elements Hf-Hg, Theor. Chem. Acc. **125**, 97 (2010).

[51] T. Fleig, J. Olsen, and L. Visscher, The generalized active space concept for the relativistic treatment of electron correlation. II. Large-scale configuration interaction implementation based on relativistic 2- and 4-spinors and its application, J. Chem. Phys. **119**, 2963 (2003).

[52] S. Knecht, H. J. A. Jensen, and T. Fleig, Large-scale parallel configuration interaction. II. Two- and four-component double-group general active space implementation with application to BiH, J. Chem. Phys. **132**, 014108 (2010).

[53] Stefan R. Knecht, Parallel Relativistic Multiconfiguration Methods: New Powerful Tools for Heavy-Element Electronic-Structure Studies, Ph.D. thesis, Heinrich-Heine-Universität Düsseldorf, 2009, http://docserv.uni-duesseldorf.de/servlets/DocumentServlet?id=13226.

[54] M. Denis, M. S. Nørby, H. J. A. Jensen, A. S. P. Gomes, M. K. Nayak, S. Knecht, and T. Fleig, Theoretical study on ThF$^+$, a prospective system in search of time-reversal violation, New J. Phys. **17**, 043005 (2015).